COMPDYN 2009
ECCOMAS Thematic Conference on
Computational Methods in Structural Dynamics and Earthquake Engineering
M. Papadrakakis, N.D. Lagaros, M. Fragiadakis (eds.)
Rhodes, Greece, 22–24 June 2009

R&D ON CONTROL OF VIBRATIONS UNDER COVICOCEPAD DURING 2007-2008

R.C. Barros[1], A. Baratta[2], O. Corbi[2], M.B. César[1], I. Corbi[2]
R. Bairrão[3], L. Guerreiro[4], C. Oliveira[4], G. Magonette[5]

[1] FEUP – Faculdade de Engenharia, Universidade do Porto (UP), Portugal
Department of Civil Engineering, Rua Roberto Frias, 4200-465 Porto, Portugal
e-mail: rcb@fe.up.pt , dec05002@fe.up.pt

[2] University of Naples Federico II, Naples, Italy
Department of Structural Engineering, via Claudio 21, 80125 Napoli, Italy
Alessandro.baratta@unina.it , ottavia.corbi@unina.it , Ileana.corbi@unina.it

[3] LNEC – National Laboratory of Civil Engineering
Avenida do Brasil, Lisboa, Portugal
bairrao@lnec.pt

[4] IST – Instituto Superior Técnico, Universidade Técnica de Lisboa (UTL), Portugal
Dept Civil Engng, Avenida Rovisco Pais, Lisboa, Portugal
luisg@civil.ist.utl.pt

[5] Structural Mechanics Laboratory, ELSA Unit
Institute for the Protection and Security of the Citizen (IPSC)
Joint Research Centre, 21020 Ispra, Italy
georges.magonette@jrc.it

Keywords: Control of Vibrations for Smart Structures, Semi-Active Devices, MR Dampers, TLD and Base Isolation devices, Experimental Tests on Shaking Table.

Abstract. *This paper provides information on the latest R&D within COVICOCEPAD project approved in the framework of Eurocores program. It addresses the use of TLD, base isolation devices, MR dampers and a hybrid technique using both devices together. Some results are provided associated with calibration of a MR damper at FEUP, as well as its inclusion in a small scale laboratory set-up with proper equations of motion of the controlled smart structure. An application of semi-active control technique to a bridge is outlined. Further remarks and details on future tests to be performed in LNEC shaking table, within COVICOCEPAD project, are provided.*

1 INTRODUCTION

In the last two decades R&D of structural vibration control devices for buildings and bridges has been intensified to reply to construction market needs that demand more effective systems to decrease the damage caused by seismic and wind loading. This orientation is the result of a public necessity to guarantee the serviceability of construction lifelines throughout and after the occurrence of a moderate or severe seismic event (Barros *et al* [1] [2]).

The COVICOCEPAD project earlier objectives and preliminary works, on TLD's and on algorithm strategies for semi-active control, have already been reported by Barros [3] [4], Barros and Corbi [5] [6], Guerreiro, Barros and Bairrão [7], among others [8] [9] [10] [11].

Herein in the sequel of contract and financial support only initiated in November 2007, which only then allowed organized contacts for potential researchers and the warranted request for the supply of a Quanser shake table II (QST-II) delivered in November 2008, the project leader and the local team coordinators synthesize part of the ongoing R&D in the project thematic. The QST at FEUP (Porto) was calibrated, from Dec 2008 until March 2009, with the adequate use of the supplied 2-DOF frame equipped with 2 passive/active TMD devices. Future collective work will detail experimental results obtained with QST at FEUP and their analytical modelling, also theoretical developments at both University of Naples (Federico II) and IST (Lisbon), as well as larger scale tests using vibration damper devices at a LNEC (Lisbon) steel frame under the same project.

2 PASSIVE, SEMI-ACTIVE AND HYBRID CONTROL OF STRUCTURES

2.1 Passive Control using Base Isolation (BI)

In the last two decades R&D of structural vibration control devices for buildings and bridges has been intensified to reply to the construction market needs that demand more effective systems to decrease the damage caused by a seismic and wind loading. This orientation is the result of a public necessity to guarantee the serviceability of construction lifelines after and throughout the occurrence of a moderate/severe seismic event.

In this context, the strategies based on the passive control, namely the base isolation (BI) systems, shock absorbers (SA) and tuned mass dampers (TMD) are well-known and accepted methodologies due to its effectiveness as mitigation approach for dynamic loading. However, the limitations that these devices/methodologies have to allow variations of the dynamic loading or structural parameters encouraged the study and development of more advanced control systems based on active, semi-active or hybrid control devices (Figure 1).

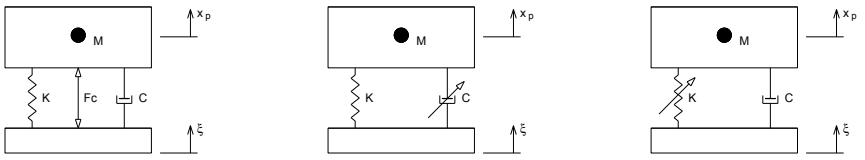

Figure 1: Active and semi-active vibration control strategies.

The numerical models used to simulate this new type of control in civil engineering structures allows to conclude that is possible to apply them successfully but some experimental research is requested to validate these models in order to be accepted as a possible structural vibration control solution. Since active devices are not a practical and reliable option in the near future as a structural building or bridge control systems due to energy demand and possible failure in case of power loss, semi-active control devices gain significant attention by the civil engineering community in the last years because they have at the same time the benefits of passive and active devices without requiring a huge amount of energy to properly work.

The easiest and cheapest way to protect a structure from undesired vibration is to add a passive isolation system to reduce the response in some sensitive region. Figure 2 shows a single degree-of-freedom isolator, modelled by the transmissibility transfer function:

$$T = \frac{x_p}{x_b} = \frac{\dot{x}_p}{\dot{x}_b} = \frac{\ddot{x}_p}{\ddot{x}_b} = \frac{1 + 2\xi_p \frac{s}{\omega_n}}{1 + 2\xi_p \frac{s}{\omega_n} + \frac{s^2}{\omega_n^2}} \tag{1}$$

where s is the Laplace variable, ω_n is the natural frequency, ξ is the passive damping ratio, x_p and x_b are the payload and base displacements. The transmissibility modulus and phase for several damping ratios are also shown in Figure 2. In this figure is visible that at low passive damping ratios, the resonant transmissibility is relatively large while at frequencies above resonant peak is quite low and the reverse is true for relatively high damping ratios.

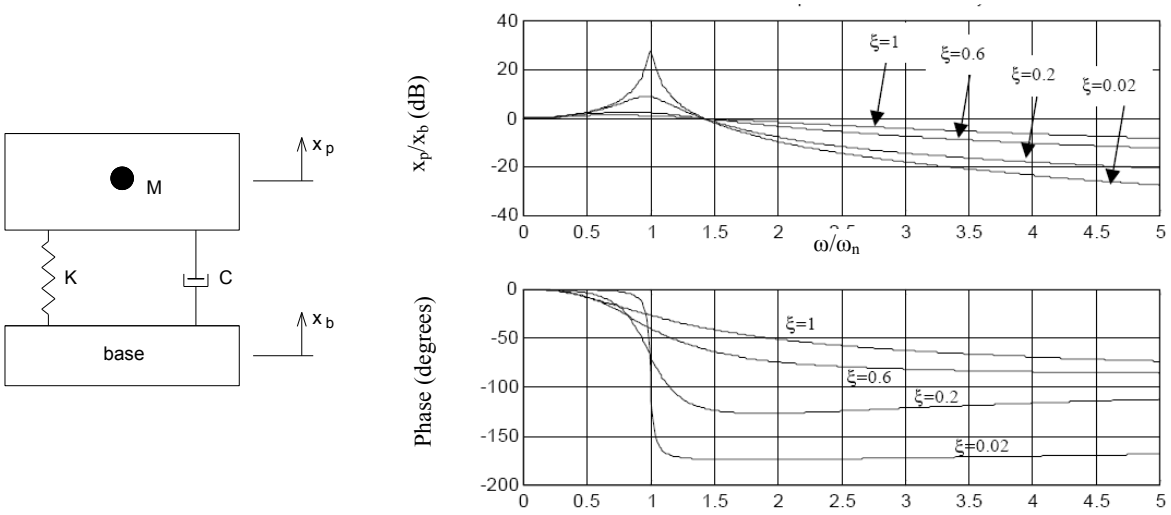

Figure 2: Passive 1-DOF isolator and transmissibility transfer function.

The base isolation system is the first approach in the analysis of structures with passive energy dissipation devices and is based on the use of a model with 2 (translational) DOF represented in Figure 3. The background to this work was based on Naeim and Kelly [12] and Soong and Dargush [13] that resumes the theory of seismic isolation and the design of seismic isolated structures, within the framework of existing codes. In this context such model was used earlier by Barros and Cesar [14] , Cesar and Barros [15]. Also Figueiredo and Barros [16] have addressed the importance of the influence of increasing damping in seismic isolation.

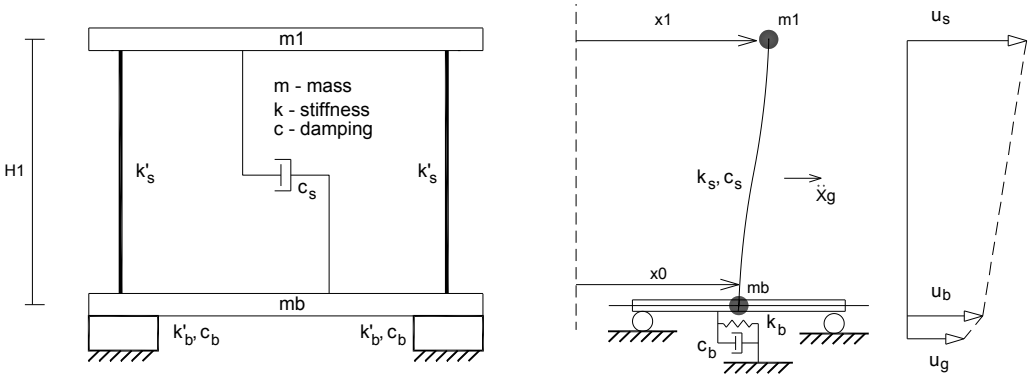

Figure 3: Passive energy dissipation at the base of the structure (Base Isolation).

The classical design approach for the base isolation devices accounting horizontal seismic component is also shown in Figure 3. In this case the equation of motion (2) has the matrix identifications (mass, damping and stiffness matrices) given in equation (3), where c_b is the damping coefficient of the isolation system, c_s is the damping coefficient of the fixed structure and k_s is the stiffness of the fixed-base structure.

$$M\ddot{X}(t)+C\dot{X}(t)+KX(t)=-M\{I\}a(t) \tag{2}$$

$$M=\begin{bmatrix} m_b & 0 \\ 0 & m_1 \end{bmatrix},\ C=\begin{bmatrix} c_b+c_s & -c_s \\ -c_s & c_s \end{bmatrix},\ K=\begin{bmatrix} k_b+k_s & -k_s \\ -k_s & k_s \end{bmatrix} \tag{3}$$

Base isolation devices are made of natural rubber that guarantees damping ratios in the order of 10-20% of critical damping, considerably bigger than structural damping ratios for steel frames (in the order of 2%). In our study a vibration absorbing mounting similar to those used for machine isolation is used to simulate the base isolation system. Because this simplified passive system has an insignificant energy dissipation – an important characteristic for real building applications – the expected structural behaviour remains the same as for a real base system; so the main purpose of a base isolation system is to increase the structural flexibility and consequently the main period to a more secure range, in which resonance effects are significantly lower (and often irrelevant) becoming a type of pseudo-filter [2] [14] [15].

Actually the final skill of base-isolation devices for structural applications in mitigating inertia forces due to intense earthquakes, strongly depends on the proper calibration of the isolator own frequency, which should be carefully dimensioned taking into account both the dynamical characteristics of the superstructure and the frequency content of the expected disturbance (Baratta and Corbi [17] [18]). Surface layers of the ground on which the building is founded have the capacity of filtering the incoming dynamic excitation making its signal dependent on the characteristics of the soil.

Therefore, in designing a base isolator system, one should not neglect the interaction effects between the structure itself and the soil characterizing the site, since the soil behaves like a filter as regards to the incoming seismic excitation, mainly affecting its frequency composition and, definitively, its overall dynamic character.

At the Department of Structural Engineering of the University of Naples Federico II, a strategy for designing an effective isolation device on the basis of the knowledge of the structure mechanical characteristics and of the soil properties has been developed, imposing that the desired isolator behaviour is such to minimize the energy introduced in the structure by the dynamic excitation, while allowing a bounded energetic absorption in the isolator itself, lower than a prefixed threshold.

The adoption of this approach requires, of course, the evaluation of the energies characterizing the structure $\mathcal{E}_{str}(\omega|\eta,\xi)$ and the base isolation device $\mathcal{E}_{is}(\omega|\eta,\xi)$ during the seismic motion, as functions of the varying isolator characteristics m_{is}, c_{is}, k_{is}, and of the soil properties η and ξ; these energies can be obtained by referring to the integrals of the relevant auto-spectral density terms.

The search of the isolator parameters can be pursued by requiring that the energy absorbed by the structure is minimum while the energy introduced in the isolator is kept bounded, by setting up the problem

$$\begin{aligned} &\text{Find} \quad \min_{m_{is}, c_{is}, k_{is}} \mathcal{E}_{str}(\omega \mid \eta, \xi) \\ &\text{Sub} \quad \begin{cases} \mathcal{E}_{is}(\omega \mid \eta, \xi) \le \overline{\mathcal{E}}_{is} \\ m_{is} \ge \overline{m}_{is} \end{cases} \end{aligned} \tag{4}$$

In Equation (4) one can observe the presence of two constraints, one being the mentioned bound on the isolator energy absorption $\overline{\mathcal{E}}_{is}$, the other being a practical bound on the minimum value of the isolator mass $\overline{m}_{is}$. Numerical investigation developed at the University of Naples on base isolated shear-type structures, subject to accelerations compatible with the Kanai-Tajimi spectra with assigned parameters η and ξ, allow to observe that in the cases when the soil is already very soft (mean square ratio higher than one) or poorly stiff (mean square ratio approximately one) with comparison to the structure, the isolator is not useful.

In Figure (4) one reports the time response of the optimal isolator $x_1(t)$ and of the optimally isolated superstructure $x_2(t)$, for a base isolated SDOF shear frame subject to a base acceleration compatible with a Kanai-Tajimi spectrum with parameters η=5 sec^{-1} and ξ=3.

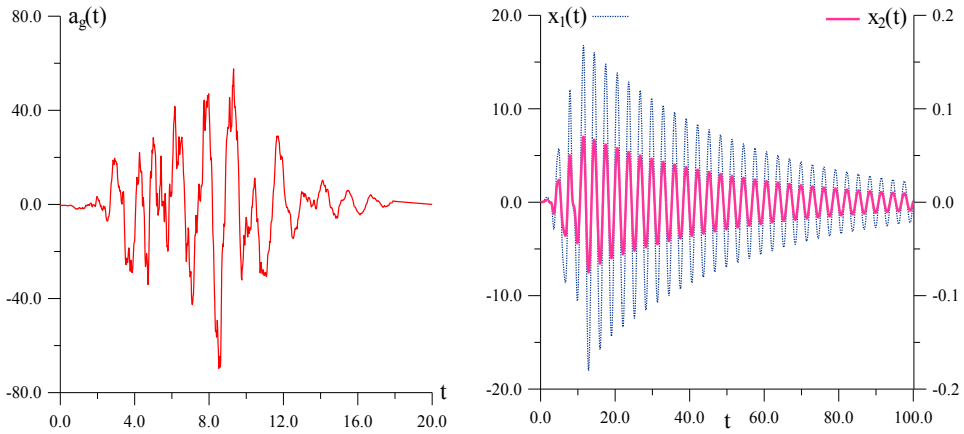

Figure 4: (a) Base acceleration compatible with the Kanai-Tajimi spectrum with η=5 sec^{-1} and ξ=3. (b) Time response of the isolated structural system.

Synthetic results on the same structure while varying the isolator mechanical characteristics in terms of ω_1 and ζ_1 are diagrammed in Figure (5), where the maximum response values attained by the isolation device and by the superstructure are reported.

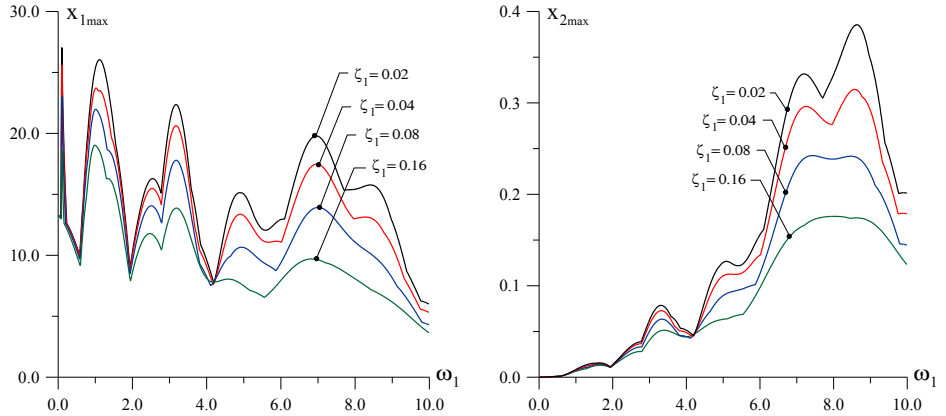

Figure 5: Curves of the maximum drifts attained during the motion by varying isolator parameters ω_1 and ζ_1: (a) isolator; (b) superstructure.

2.2 Passive Control using Tuned Liquid Dampers (TLD)

Among the many vibration control devices available to increase the damping characteristics of the structures, tuned liquid dampers (TLD) offer several advantages, namely: low cost, easiness to install in existing structures and effectiveness even for small-vibrations (Kareem [19], Corbi [20], Barros and Corbi [5] [6], Barros [21]).

The performance of TLD relies mainly on the sloshing of liquid at resonance to absorb and dissipate the vibration energy of the structure. The liquid is contained in partially filled tanks mounted on the structure. The shear force F_{TLD} caused by the inertia of the liquid mass reduces the structural response due to the excitation action F_g (Figure 6).

Tuning the natural frequency of liquid sloshing with the natural frequency of structure, results in the optimization of the effectiveness of the damper.

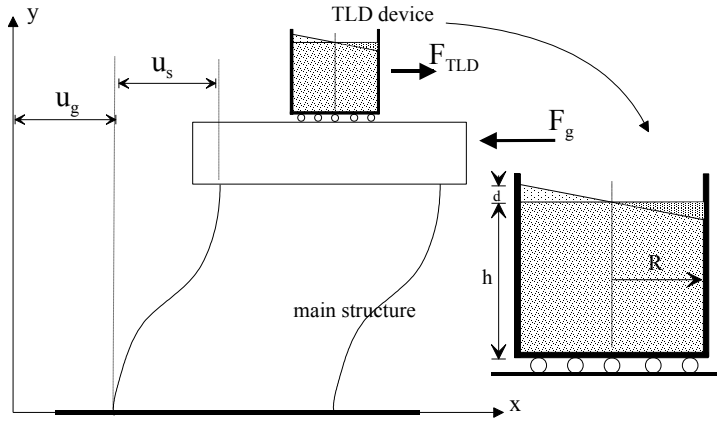

Figure 6: SDOF shear frame equipped with TLD device.

Theoretical models of liquid sloshing in TLD can be obtained either from a mechanical analogue, or from more exact analytical models of the structural and liquid domain. Actually the reliable prediction of dynamic response of control devices based on fluid motion plays a central role for better understanding the real perspectives offered by TLD for applications in the field of intelligent structures, as regards to mitigation of earthquake and vibration hazards through vibration control.

The need of predicting and preventing failures associated to rocking and overturning of rigid structures undergoing strong ground shaking have motivated a consistent number of studies on rocking response of rigid blocks, and the possibility of coupling sloshing devices for attenuating their rocking response to dynamic excitations appears pretty interesting.

Laboratory tests developed at the Laboratory of the Department of Structural Engineering of the University of Naples on metallic blocks (Figure 7) equipped with sloshing dampers prototypes and located on a shaking table show the potential benefits produced by these devices in attenuating the primary model response (Kareem [19]). Experimental data in Figures 8-10 show that significant beneficial effects can be produced in the attenuation of the rocking motion; this is quite clear, for example, from the diagram of the curves depicting the empty/full ratio for the model equipped with a trapezoidal tank (Figure 7): the ratio between the model responses for the empty tank and for the tank filled with 4 cm or 8 cm of water shows the performance of the device, whose effectiveness is mainly lumped on a given frequency range. As it appears, the level of the liquid in the tank is able to deeply change the characteristics of the device and, therefore, its overall response.

The effectiveness of the device can be appreciated by comparison with the unit-ratio line. Time histories also confirm the advantage of adopting such devices in the considered frequency range, showing a good mitigation of the dynamical response of the primary model.

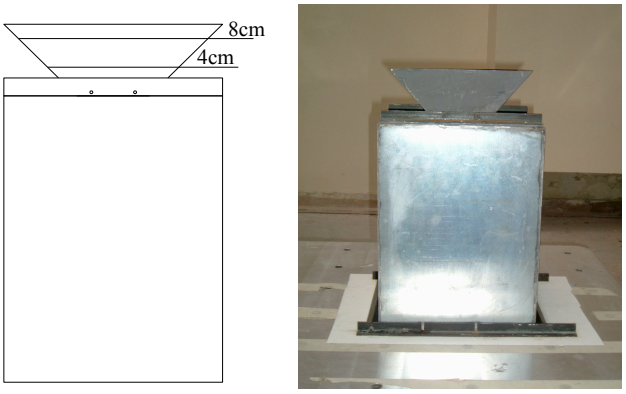

Figure 7: Block equipped with 45° tank marked at two liquid levels (4cm and 8cm).

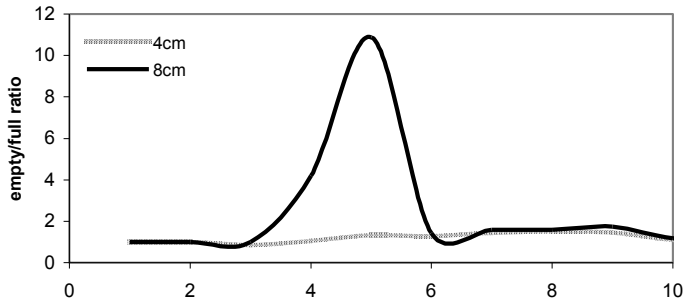

Figure 8: Block 30×30×40 cm equipped with a trapezoidal tank.

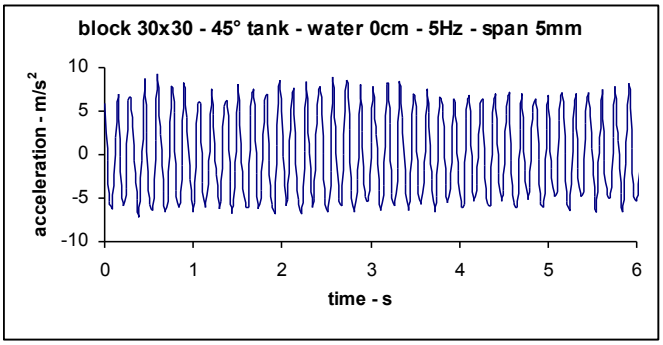

Figure 9: Block 30×30×40 cm equipped with a trapezoidal (45°) empty tank.

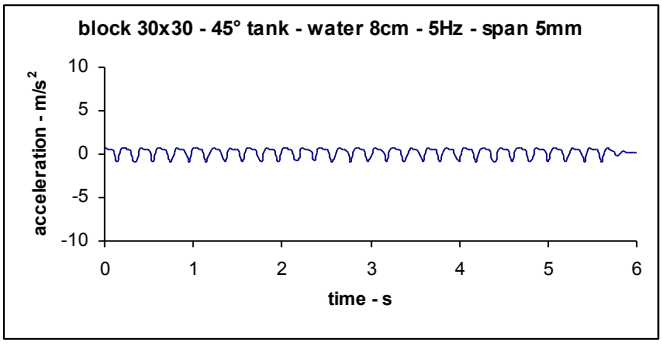

Figure 10: Block 30×30×40 cm equipped with a trapezoidal (45°) tank filled with 8cm of water.

2.3 Semi-Active Control

The next step is to use semi-active devices to control the vibration of a base excited structure. Among the possible semi-active technologies, the magneto-rheological fluid based devices are seen as a promising solution for structural control.

Basically two types of rheological fluids can be used to create a structural control system: Magneto-rheological (MR) and Electro-rheological (ER) fluids. MR fluids are materials that exhibit a change in rheological properties with the application of a magnetic field while ER fluids exhibit rheological changes when an electric field is applied to the fluid.

Although power requirements are approximately the same MR fluids only require small voltages and currents while ER fluids require very large voltages and very small currents. However, ER fluids have many disadvantages including relatively small rheological changes and significant property changes with temperature. Thus, MR fluids have become an extensively studied "smart" fluid and some experimental research has been done in the last years to produce a "smart" control device with this fluid.

Usually, the MR fluid devices are built to operate in the following modes (Figure 11): valve mode or flow mode; direct shear mode or clutch mode; squeeze film compression mode and the combination of some of the previous modes.

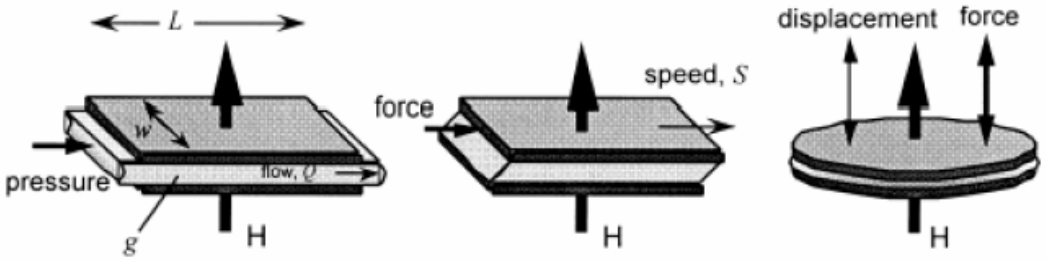

Figure 11: Basic operation modes of MR-fluid.

For vibration control purposes the "smart" MR fluid effect is interesting since it is possible to apply this phenomenon to create a variable damping device or a "smart" hydraulic damper. The current applied to a MR fluid essentially allows controlling the damping force without the need of mechanical valves that are commonly used in adjustable dampers. This offers the possibility to create a reliable damper since a failure in the control system reverts the MR damper to a passive damper (Figure 12).

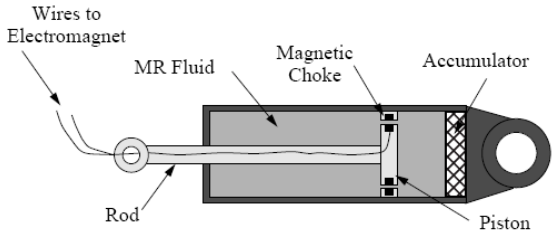

Figure 12: Schematic representation of a magneto-rheological damper.

The MR damper performance is often characterized by using the force vs. velocity relationship. Regular viscous damper has an ideal linear constitutive behaviour and the slope of the line is known as the damper coefficient. In the case of MR dampers the possibility to change the damping characteristics leads to a force vs. velocity envelope that can be described as an area rather than a line in the force-velocity plane. This behaviour is the fundamental

condition to build a "smart" damper since it is possible to design a controller to follow any force-velocity relationship within the envelope to create a control strategy.

According to the available bibliography two common methods can be used to model MR devices such as MR dampers: the parametric modelling technique that characterizes the device as a collection of springs, dampers, and other physical elements; the non-parametric modelling that employ analytical expressions to describe the characteristics of the modelled devices. Many authors have developed modelling techniques for the MR dampers based on both methods. In recent studies Dyke *et al* [22] presented a simple parametric model based on the extension of the Bouc-Wen model that allows a good approximation to the real MR damper behaviour as shown in Figure 13.

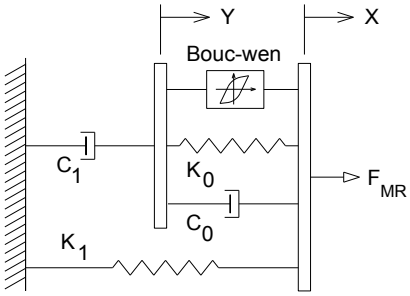

Figure 13: Modified Bouc-Wen model for a MR damper.

The Bouc-Wen model is based on the Markov-vector formulation to model nonlinear hysteretic systems and according with the modified model shown in Figure 13, the MR force can be computed by

$$F_{MR} = c_1 \dot{y} + k_1 \left(x - x_0 \right) \tag{5}$$

$$\begin{cases} \dot{y} = \dfrac{1}{\left(c_0 + c_1 \right)} \left\{ \alpha z + c_0 \dot{x} + k_0 \left(x - y \right) \right\} \\ \dot{z} = -\gamma \left| \dot{x} - \dot{y} \right| z \left| z \right|^{n-1} - \beta \left(\dot{x} - \dot{y} \right) \left| z \right|^{n} + A \left(\dot{x} - \dot{y} \right) \end{cases} \tag{6}$$

In these equations z is the revolutionary variable, F_{MR} is the predicted damping force, k_1 is the accumulator stiffness, c_0 is the viscous damping observed at larger velocities and the parameters β, γ and A allows controlling the linearity in the unloading and the smoothness of the transition from the pre-yield to the post-yield region. The dashpot c_1 is included to produce the roll-off at low velocities, k_0 is used to control the stiffness at larger velocities, and x_0 is the initial displacement of spring k_1 associated with the nominal damper due to the accumulator.

$$\begin{cases} c_1 = c_{1a} + c_{1b} u \\ c_0 = c_{0a} + c_{0b} u \\ \alpha = \alpha_a + \alpha_b u \\ u = -\eta \left(u - v \right) \end{cases} \tag{7}$$

The damping constants c_0 and c_1 depend on the electrical current applied to the MR damper. The variable u is the current applied to the damper through a voltage-to-current converter with a time constant η and the variable v is the voltage applied to the converter.

A simple MATLAB/SIMULINK block diagram can be used to simulate the Bouc-Wen model of a MR damper as shown in Figure 14.

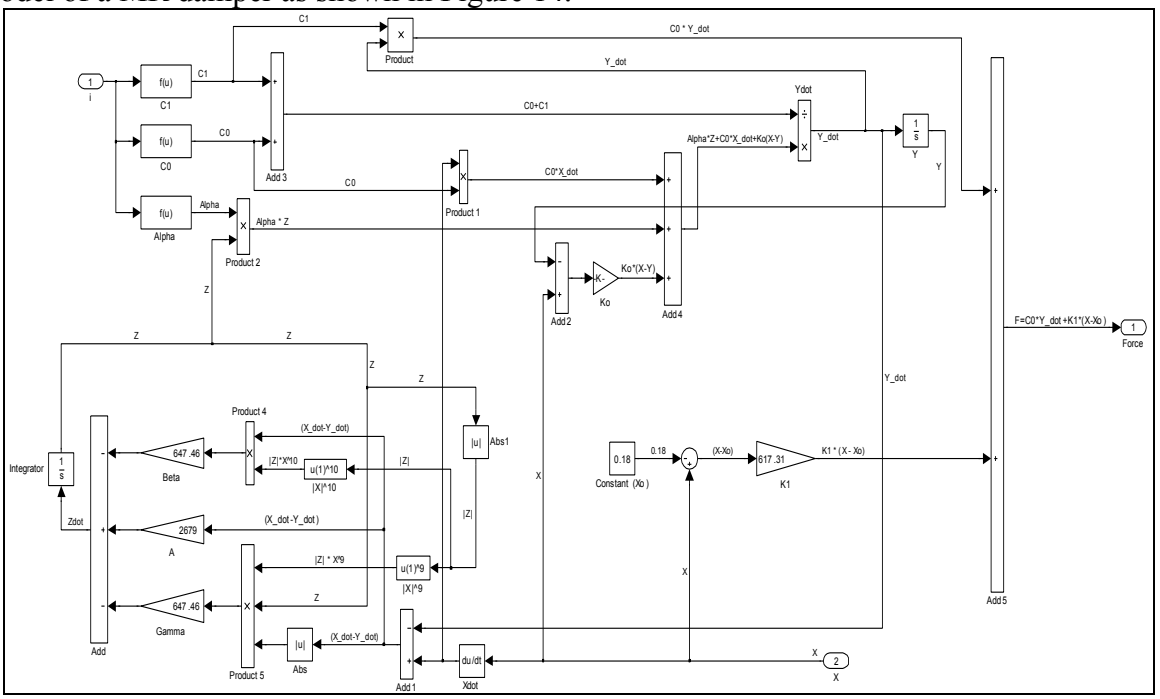

Figure 14: Block diagram of a Magneto-rheological damper using a Bouc-Wen model.

To study the behaviour of a MR damper some experiments were carried out on a MTS universal testing machine, of the Mechanical Engineering Laboratory at FEUP, with the MR damper device RD-1005-3 supplied by LORD Corporation (Figure 15).

According to the device specifications it has a capacity to provide a peak to peak force of 2224 N at a velocity of 51 mm/s with a continuous current supply of 1 A. The MR damper was tested using the computer-controlled servo hydraulic MTS universal testing machine shown in Figure 16. The MR damper was attached to the MTS machine (operating under displacement control mode) and a 5 kN load cell was incorporated at the upper head to measure the force applied to the damper. The results were automatically collected by the computer-controlled MTS equipment and stored in a desktop PC.

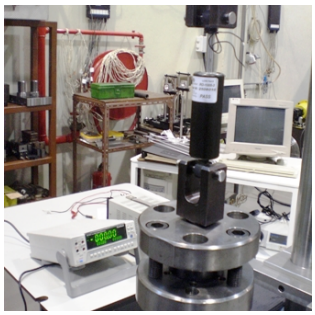

Parameter	Value
Extended length	208mm
Device stroke	±25mm
Max. Tensile force	4448N
Max. temperature	71ºC
Compressed length	155mm
Response time	<10ms
Max. Current supply	2A

Figure 15: Magneto-rheological damper RD-1005-03 test setup at FEUP.

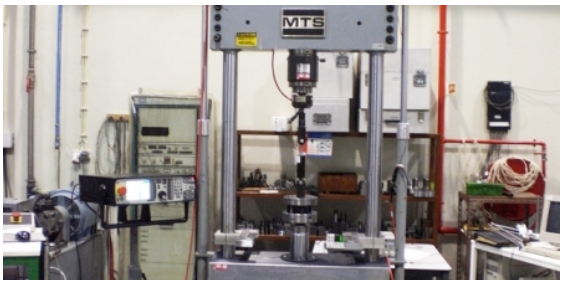

Figure 16: Magneto-rheological damper with current supply device, connected to MTS universal setup (FEUP).

After assemblage, the MR damper was forced with a sinusoidal signal at a fixed frequency, amplitude and current supply. To obtain the response of the MR damper under several combinations of frequencies, amplitudes and current supplies a series of tests were carried out. Therefore, a set of frequencies (0.5, 1.0, 1.5 and 2.0 Hz), amplitudes (2, 4, 6, 8 and 10 mm) and current supplies (0.0, 0.1, 0.2, 0.25, 0.5, 0.75, 1.0 and 1.5 A) were used to complete the test program. In order to control and avoid temperature failure, especially at higher frequencies, a thermocouple was used to measure the external temperature of the MR damper. Typical results of this experimental research are shown in Figures 17 and 18.

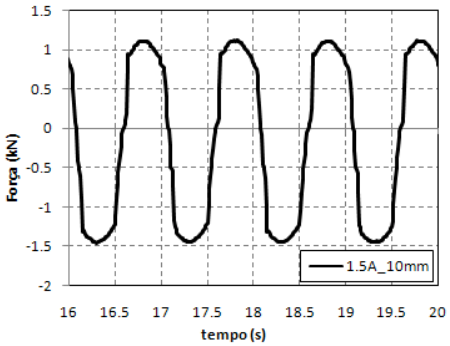

Figure 17: MR damper RD-1005-03 Force-Time History (1.5 A and 10mm).

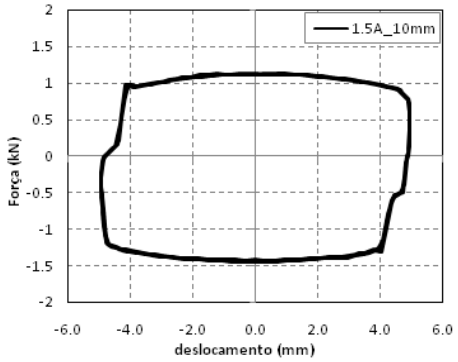

Figure 18: MR damper RD-1005-03 Force-Displacement curves (1.5 A and 10mm).

The variable current tests demonstrate that increasing the input current implies an increase in the force required to yield the MR fluid and a plastic-like behaviour in observed in the hysteretic loop. In the frequency dependent test is observed that the maximum damping force increases with the frequency due to large plastic viscous force at higher velocity.

According with the scheduled research program the next step will be to study the experimental dynamic behaviour of a scaled metallic load frame with passive and semi-active devices, namely MR dampers (Figure 19).

This frame will be tested at the FEUP-Covicocepad Lab using the QUANSER shaking table II shown in Figure 20 as the dynamic loading actuator.

The experimental research employs three control strategies: (1) a passive control based on base isolation devices; (2) a semi-active control based on a MR damper assembled to the structure; (3) a hybrid control technique through the association of the base isolation devices with the MR damper.

To study the semi-active control strategy a MR damper is placed at the first floor level attached to the frame and rigidly attached to the shaking table. The structure is excited using the N-S component of the 1940 El Centro earthquake as the seismic ground acceleration, time-scaled with Froude similarity according to the shaking table model, in order to obtain the frequency characteristics of the structure and the physical model parameters.

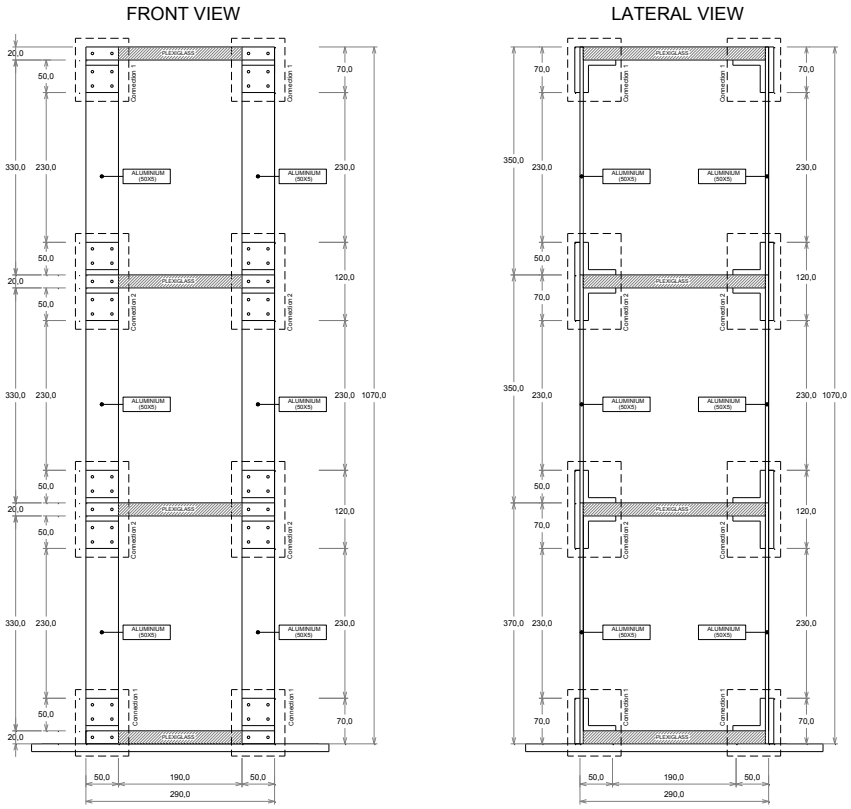

Figure 19: 3-DOF small metallic frame at FEUP – Covicocepad Lab.

Figure 20: Quanser shaking table II (and its controllers) at FEUP – Covicocepad Lab.

The equation of motion that describes the behaviour of a controlled building under an earthquake load is given by:

$$M\ddot{x} + C\dot{x} + Kx = -\Gamma f - M\lambda\ddot{x}_g \tag{8}$$

where M is the mass matrix, C is the damping matrix, K is the stiffness matrix, x is the vector of floors displacements, $\dot{x}$ and $\ddot{x}$ are the floor velocity and the acceleration vectors respectively, f is the measured control force, λ is a vector of ones and Γ is a vector that accounts for the position of the MR damper in the structure.

This equation can be rewritten in the state-space form as

$$\dot{z} = Az + Bf + E\ddot{x}_g \tag{9}$$

$$y = Cz + Df + v \tag{10}$$

where z is the state vector, y is the vector of measured outputs and v is the measurement noise vector. The other variables are defined by

$$\begin{aligned} A &= \begin{bmatrix} 0 & I \\ -M^{-1}K & -M^{-1}C \end{bmatrix} \qquad B = \begin{bmatrix} 0 \\ M^{-1}\Gamma \end{bmatrix} \quad E = -\begin{bmatrix} 0 \\ \lambda \end{bmatrix} \\ C &= \begin{bmatrix} -M^{-1}K & -M^{-1}C \\ I & 0 \end{bmatrix} \qquad D = \begin{bmatrix} M^{-1}\Gamma \\ 0 \end{bmatrix} \end{aligned} \tag{11}$$

To control this semi-active structure based on a control force determination, usually are measured: the absolute acceleration of some relevant selected points in the structure; the displacement of the control device; and the control force.

2.4 Control algorithms

After calibrating the MR damper numerical model it is necessary to select a proper control algorithm to efficiently use this device in reducing the dynamic response of structural systems. Obviously, the control strategy depends on the MR damper model selected to simulate the nonlinear hysteretic behaviour of this device (Jansen and Dyke [23], Kang-Min *et al* [24]).

The fundamental condition to operate the MR damper is based on a generated damping force that is related with the input voltage; the control strategy is selected so that the damping force can track a desired command damping force. The available models can be categorized in static and dynamic models. The basic difference between them is that the static models do not include dynamic relation between input and output.

As mentioned before this work is based on the Bouc-Wen model that can represent the hysteresis dynamics explicitly. Therefore, an efficient control algorithm must be developed or chosen from the available research bibliography to correctly characterize the intrinsic MR fluid behaviour, maximizing the MR damper characteristics as a semi-active control device.

In the last few years several approaches have been proposed and intensively studied for better selection of the input voltage that must be applied to the MR damper to achieve the maximum performance. Among the proposed strategies the following are the most studied: Lyapunov Based Control; Decentralized Bang-Bang Control; LQG (Linear Quadratic Gaussian) or Clipped-Optimal Control; H_2/LQG control; Fuzzy Control and also Artificial Neural Network (ANN) control strategies. Some of these control strategies will be applied in this research program in order to understand the pros and cons of each strategy. After performing an exhaustive study on the numerical model and small mock-up experimental model, the more reliable vibration control algorithms will be applied to medium-scale experimental models.

2.4.1 *Clipped-Optimal Control*

A semi-active clipped-optimal control based on acceleration feedback was proposed by Dyke *et al*. [22]. The control diagram of this control strategy is shown in Figure 21.

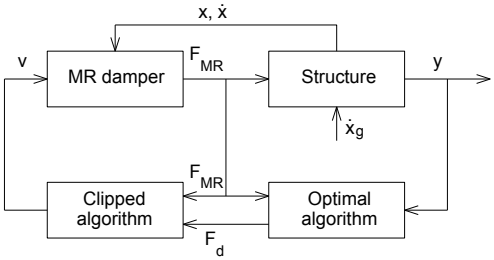

Figure 21: Semi-active clipped-optimal control diagram.

As shown in the diagram this strategy has two controllers and is based on a linear optimal controller designed to set the command signal to zero or to the maximum level. The signal is selected according with the desired command force, and the comparison between this force and the effective MR damper force. In this case, the command signal can be computed as

$$F_{MR} = \begin{cases} F_d, & F_d \cdot \dot{x}_{dev} < 0 \\ 0, & otherwise \end{cases} \tag{12}$$

where F_{MR} is the control force of the MR damper and $\dot{x}$ is the velocity across the damper.

2.4.2 *Fuzzy Control*

One of the recent semi-active control strategies is based on the fuzzy control inference. As shown in Figure 22, this strategy has only one controller.

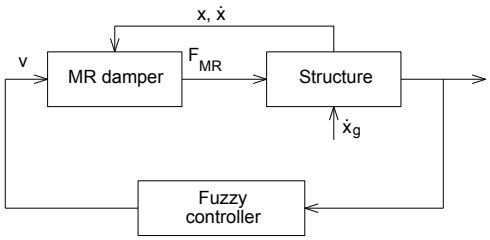

Figure 22: Semi-active clipped-optimal control diagram.

The fuzzy algorithm is used to compute the command signal and the voltage is selected using a fuzzy rule inference. The model can much easier accommodate uncertainties of input data and structural response sensors. Also is a more reliable strategy since is fail-safe since it guarantees the bounded-input/ bounded-output stability of the controlled structure [24].

2.5 A Semi-Active Control Application to Bridges

Seismic protection of bridges involves different types of control with distinct characteristics. Semi-active control is one of the new fields of research in the area, using controllable semi-active devices that have the potential to achieve a performance close to active devices using less energy. Following an algorithm, the semi-active device is capable of modifying its dynamic characteristics in order to improve the global system response. The key factor that determines the full application of that potential is the choice of the right control algorithm (Oliveira and Guerreiro [25]; Guerreiro, Barros and Bairrão [7]).

In the scope of COVICOCEPAD a research program was performed in order to develop a set of control algorithms. In those algorithms the input force on the device depends both on the velocity and on the displacement of the bridge deck.

The force calculation is based on an algorithm that uses a special combination of displacement, velocity and control criteria causing a considerable improvement of the system response. The control algorithms were tested in a system subjected to two different actions: a simple harmonic function in resonance with the model and a generated accelerogram according to the Portuguese code.

The results obtained were compared with the no protection case and using a passive device, demonstrating the significant advantages of this semi-active control algorithm.

To evaluate the behaviour of a seismic protection in a structural system, a parameter reflecting its influence has to be included in the dynamic equation of motion. Therefore, in Equation (13), Γ corresponds to the force generated in the seismic protection device. While $\Gamma = 0$ in the situation of no protection, for different kinds of seismic protection Γ will take different functional configurations.

$$m\ddot{x}(t) + c\dot{x}(t) + kx(t) + \Gamma = F(t) \tag{13}$$

The semi-active control function developed follows Equation (14), with the functions *f* and *g* defined by Equations (15) and (16). Function *f* depends on the velocity in the time instant in analysis, on the maximum velocity response of the last 3 iterations and on the parameter F, later on discussed. In function *g*, the displacement in the time instant in analysis, the maximum displacement response of the last 3 iterations and the parameter G are joined together with the coefficient C_1. This coefficient (C_1) varies between -1 and 1, depending if the structural displacement and velocity have the same sign, as stated in Equation (17). As the algorithm was created with the purpose to be implemented in variable damping devices such as magneto-rheological devices or variable-orifice devices, in each iteration, Γ has the same sign as the term $c\dot{x}$ of Equation (13).

$$\Gamma = \frac{|f(\dot{x}) + g(x)|}{|\dot{x}|} \times \dot{x} \tag{14}$$

$$f(\dot{x}) = |\dot{x}_{\max 3}| F\dot{x} \tag{15}$$

$$g(x) = |x_{\max 3}| C_1 G x \tag{16}$$

where: $\dot{x}_{\max 3}$ is the maximum velocity response for the last 3 iterations; $x_{\max 3}$ is the maximum displacement response for the last 3 iterations; and

$$C_1 = \begin{cases} 1 & if\ x\dot{x} > 0 \\ -1 & if\ x\dot{x} \le 0 \end{cases} \tag{17}$$

The parameters F and G should be studied for each structure model in analysis and for each seismic action to be considered. These parameters allow the adjustment of the algorithm in order to improve the structural response. To the purpose of comparison with an equivalent passive situation, F and G should be such that Equation (18) is verified for every time instant.

$$\Gamma \le F_{\max Passive} \tag{18}$$

where $F_{\max Passive}$ is the maximum force of the passive device.

The velocity-dependent term (function f) of the algorithm provides a regular seismic protection similar to a damper ($F = c\dot{x}^{\alpha}$), having the maximum force at the time of maximum velocity (or when displacement equals zero) and forming an elliptical shape in the Force versus Displacement chart (Figure 23). The displacement-dependent term (function g) runs in the opposite way: the force is maxima for maximum displacement (or when velocity equals zero), as seen in Figure 24. It implies that this term completes the elliptical shape referred, turning the sum into a rectangle (Figure 25), which results in maximizing the dissipation cycle and consequently reducing the structural response.

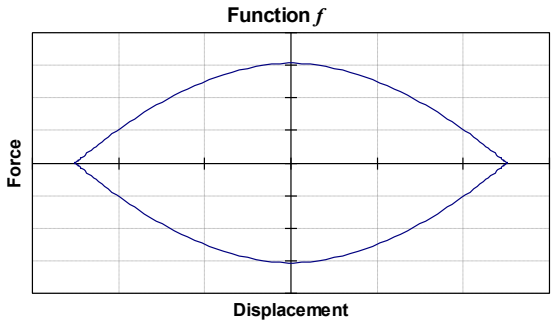

Figure 23: Force vs. Displacement of function $|f(\dot{x})| \times \frac{\dot{x}}{|\dot{x}|}$

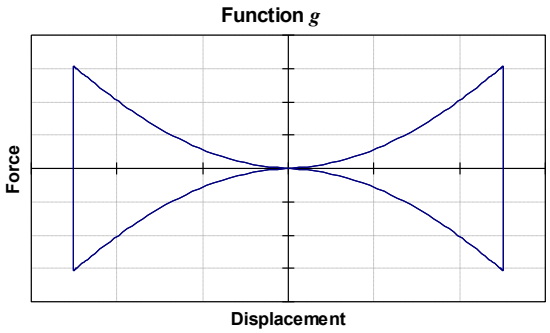

Figure 24: Force vs. Displacement of function $|g(x)| \times \frac{\dot{x}}{|\dot{x}|}$

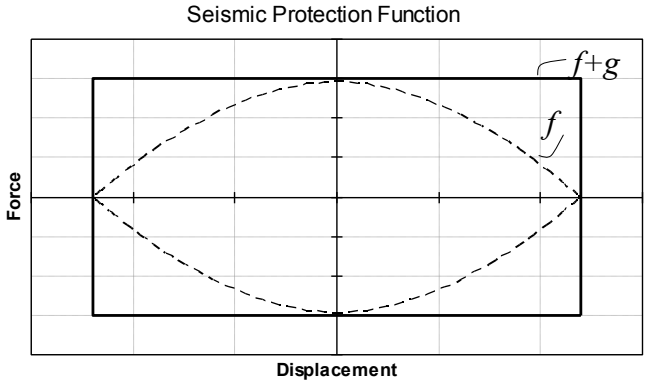

Figure 25: Force vs. Displacement of function Γ

In Figure 26 is represented the comparison between the seismic response of a viaduct located in the southern region of Portugal, with and without control. In the semi-active control device, four different sets of characteristic values were tested for the studied control algorithms (Oliveira [26]).

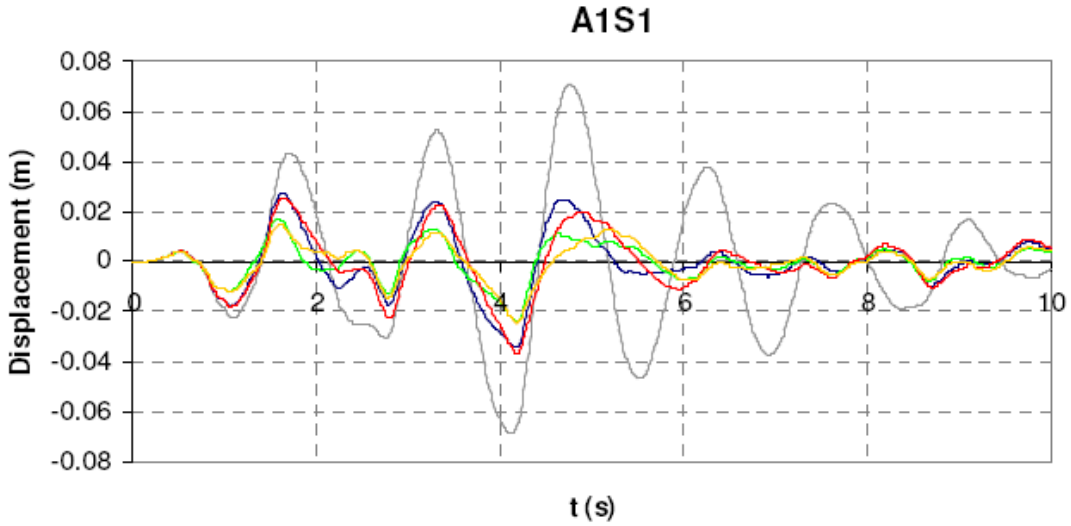

Figure 26: Comparison between the semi-active control and no protection seismic response.

3 STEEL FRAME AVAILABLE FOR THE SHAKING TABLE TESTS AT LNEC

As before mentioned, the small scale frame in Figure 19will be tested as a small mock-up structure at the QST of FEUP-Covicocepad Lab (Figure 20) to assess passive and semi-active control of vibrations methodologies and algorithms using base isolation and MR devices.

With such acquired experience, further structural vibration tests foreseen for the COVICOCEPAD project will be performed at a larger scale at the LNEC shaking table; TLD and MR devices will be used and tested on a steel frame whose dynamic characteristics are already well known, because it has been fully analyzed during previous applications while studying in detail the characteristics of the LNEC shaking table [27] [28].

The structural elements of this test steel frame were designed through an elastic analysis with the finite element program SAP-2000NL for two earthquake time history accelerations, both with peak ground acceleration of 0.5g: one was a simulated earthquake according to type 1 seismic action of the Eurocode-8 [29]; and the other was the 1940 El Centro earthquake.

The El Centro time history is a low frequency shake with most of its energy in the frequency range below 8 Hz (periods above 0.125 s), hence it is suitable to test the specimen at its natural frequency; moreover this earthquake, even if is not ideally suited to the role of the standard time history, is useful to test any shaking table up to its performance limits.

In Figures 27 and 28 are plotted the 1940 El Centro time history of acceleration and the corresponding response spectrum versus natural period.

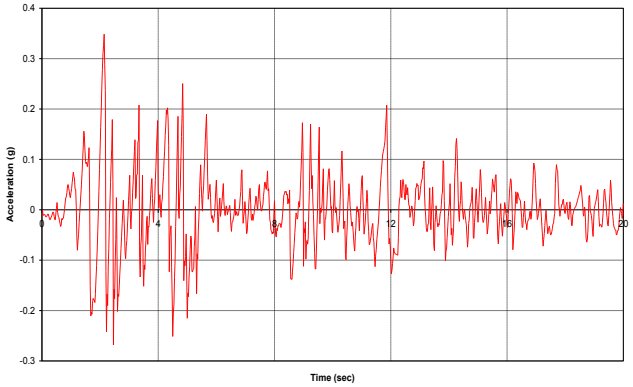

Figure 27: Acceleration time history of 1940 El Centro earthquake.

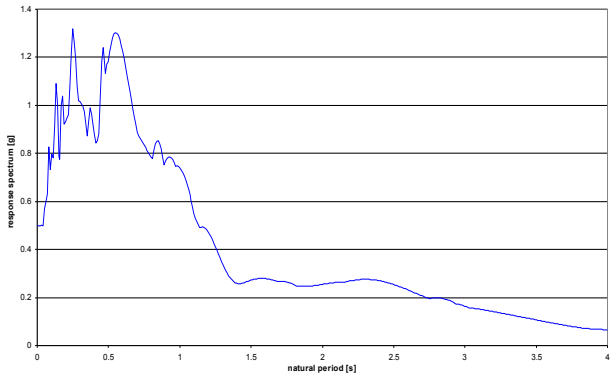

Figure 28: Response spectrum of El Centro earthquake.

On the other hand, the choice of the simulated earthquake according to type 1 seismic action of Eurocode-8 (EC-8) was justified by the will of exciting the frame with a maximum force at its natural frequency (in this case, about 8 Hz); so, for this frame, the simulated earthquake according to type 1 seismic action is more suitable than the simulated earthquake according to type 2 seismic action.

Figures 29 and 30 represent the acceleration time history for a simulated earthquake (according to type 1 seismic action of Eurocode-8) and the corresponding response spectrum.

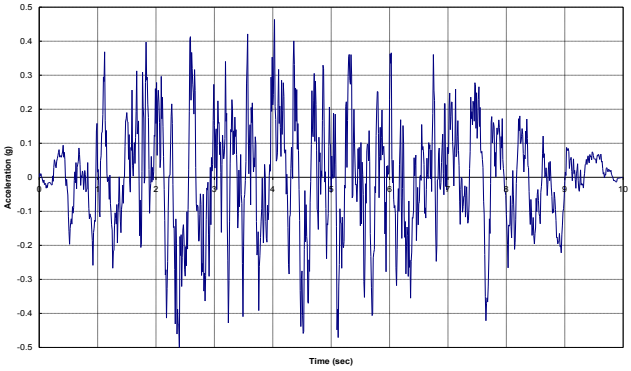

Figure 29: Time history acceleration of the simulated earthquake according to type 1 seismic action of EC-8.

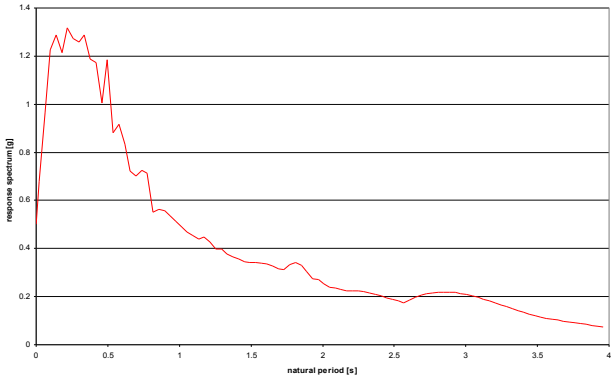

Figure 30: Response spectrum for the simulated earthquake according to type 1 seismic action of EC-8.

According to design requirements the main dimensions of the frame are given in Table 1.

	Length [m]
Inter-storey distance	3.00
Column height	4.50

Longitudinal length	3.00
Transverse length	2.75

Table 1: Main dimensions of the steel frame.

The longitudinal and transverse dimensions were chosen according to the platform limits for shaking table tests as well as the height of the column and the inter-storey distance. The slab floors can be 3 meters spaced, allowing the possibility of adding another slab floor and consequently another degree of freedom simply using structural bar elements with the same characteristics and details of the basic structure. The main dimensions of the structural elements are presented in Figure 31.

The choice of the steel sections was based on a compromise between flexibility and maximum admissible displacements during the tests, because it is necessary to have a structure with natural frequency in a useful range for experimental tests, between 6 and 20 Hz, but with bounded displacements not exceeding the imposed limit by the actuator capacity.

So columns and beams were respectively chosen as HEB 100 and HEB 180 steel sections, while the K and X braces were chosen as HEB 100 and UPN 100 sections. For the latter case the choice was imposed to allow the cross of the braces. The steel selected is of grade S355.

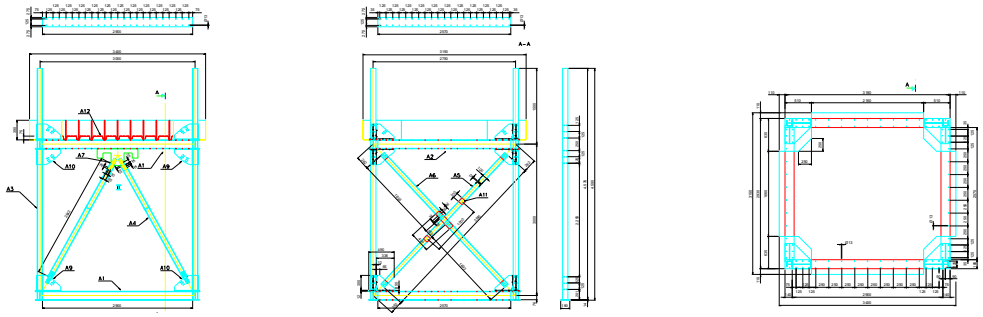

Figure 31: General overview of the specimen, plan, longitudinal and transverse overviews.

After this first choice of the main structural elements steel sections, the frame was verified through an elastic analysis with the SAP-2000NL programme, assuming the passive device with high yield strength and hence unable to dissipate energy. The maximum internal forces on the main elements through this analysis are summarized in Table 2.

Element	Axial load [kN]	Bending moment [kNm]	Shear load [kN]
Column	114.0	6.1	9.7
Beam	37.7	6.6	24.1
Longitudinal brace	100.1	0.6	0.4
Transverse brace	60.1	0.3	0.4

Table 2: Maximum internal forces on the main structural elements.

All the previously selected steel sections satisfy the demands of resistance for stresses and buckling phenomena. Further details of the elements are given in Figure 32.

The connections between the braces and the devices were verified for the maximum forces that the passive-control device bears and were ensured with bolts of grade 10.9. The connections between the braces and the base structural elements were designed with the same construction details, while the joints between the brace and column or beam plates were accomplished by welding. Some details of these connections are shown in Figure 33.

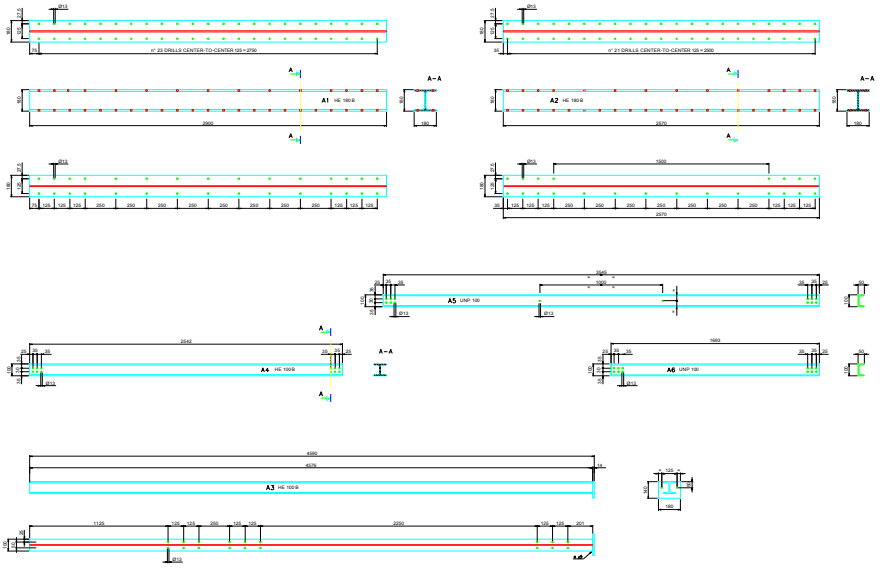

Figure 32: Details of steel structural elements: beams, columns and braces.

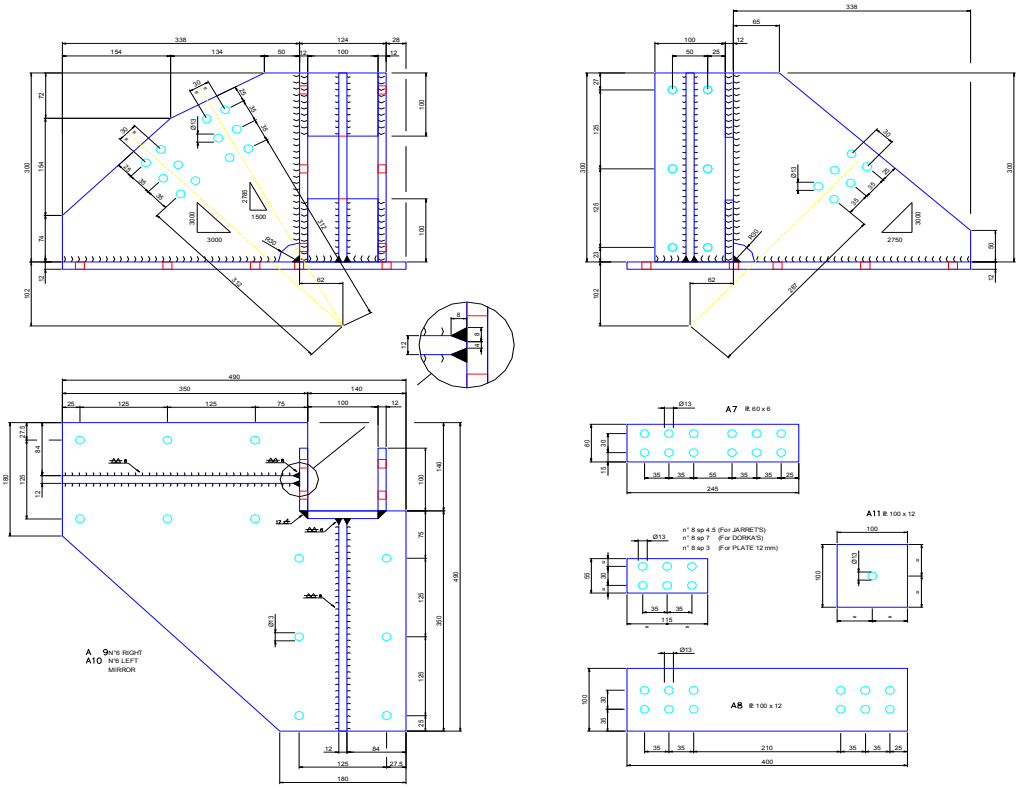

Figure 33: Details of the connections and the plates.

With this configuration, the frame weight was calculated and the choice of the thickness of the slab was made in order to reach approximately a value of 10 tons. The slab is constituted by sheet metal and concrete properly connected, but during the concrete casting the slab should be shored up to reduce the lowering of the slab in the setting phase.

The slab is shown in Figure 34 and the details of the casting are shown in Figure 35.

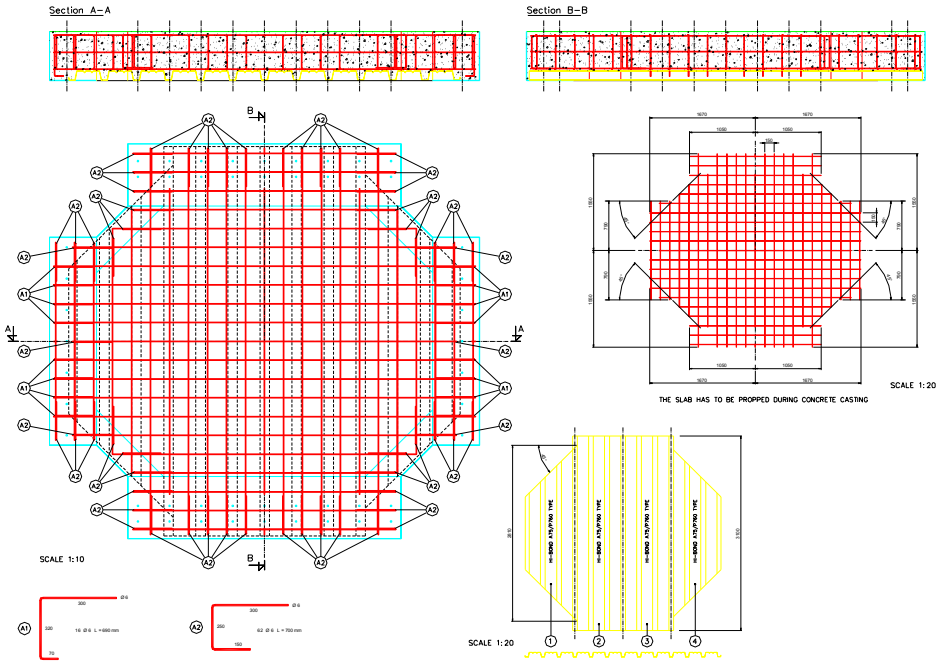

Figure 34: Plan and section views of the floor slab.

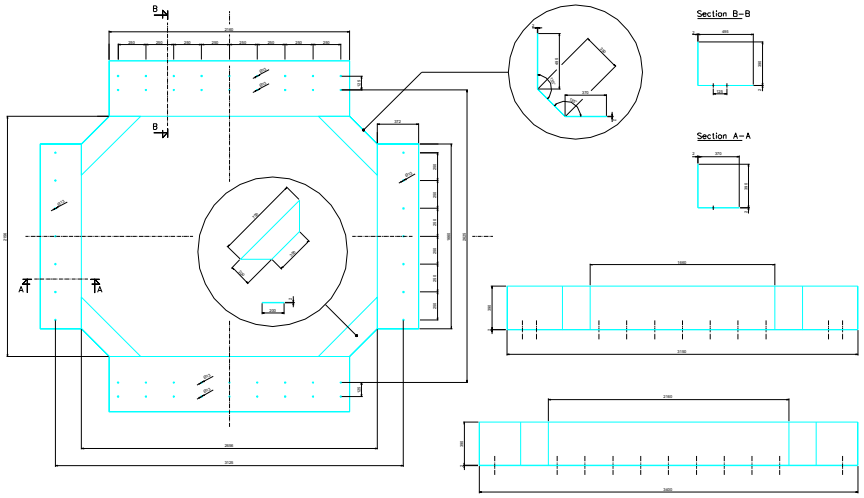

Figure 35: Casting details of the floor slab.

Figure 36 presents the real frame during the project NEFOREEE shaking table tests [28] performed earlier at the National Technical University of Athens (NTUA).

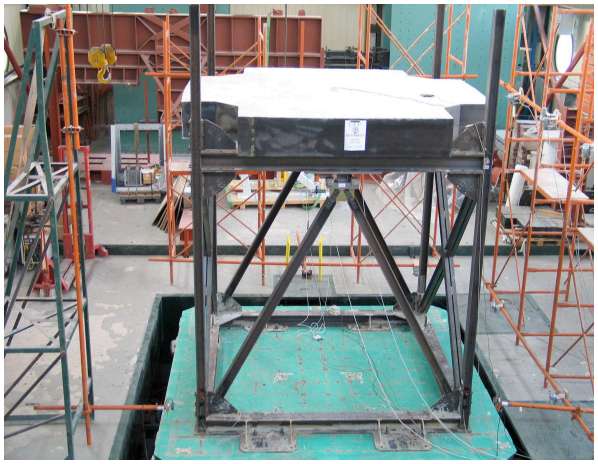

Figure 36: The steel frame during performance tests at NTUA.

ACKNOWLEDGEMENTS

This work reports research developed under the R&D Eurocores Project COVICOCEPAD within the S3T Program, approved independently by European Science Foundation (ESF, Strasbourg), financially supported by portuguese "FCT – Fundação para a Ciência e a Tecnologia" (Lisbon – Portugal) under *Programa Operacional Ciência e Inovação 2010* (POCI 2010) of the *III Quadro Comunitário de Apoio* funded by FEDER, and also by italian "CNR – Centro Nazionale della Ricerca" (Rome – Italy), under the EC Sixth Framework Program.

REFERENCES

[1] R.C. Barros, P. Belli, I. Corbi and M. Nicoletti; "Large Scale Risk Prevention", *International Journal of Earthquake Engineering and Engineering Seismology*, European Earthquake Engineering 1.04, ISSN 0394-5103, Vol. XVIII, No.1, pp. 10-19, Patròn Editore, Bologna, Italy 2004.

[2] R.C. Barros, R. Bairrão, F. Branco, I. Corbi, M. Kemppinen, G. Magonette, F. Paulet and G. Serino; "Implementation of Structural Control", *International Journal of Earthquake Engineering and Engineering Seismology*, European Earthquake Engineering 2.05, ISSN 0394-5103, Vol. XIX, No.2, pp. 51-68, Patròn Editore, Bologna, Italy 2005.

[3] R.C. Barros, "Seismic Response of Tanks and Vibration Control of their Pipelines", *Journal of Vibroengineering*, Vol. 4, 2002 - No. 1 (8), Index 136, pp. 9-16, Proceedings Research Center of the Public Institution Vibromechanika, Vilnius, Lithuania, 2002.

[4] R.C. Barros, "Project COVICOCEPAD under Smart Structural Systems Technologies of Program Eurocores"; World Forum on Smart Materials and Smart Structures Technologies (SMSST-2007) Chonqing and Nanjing (China), 22-27 May 2007; in: *Smart Materials and Smart Structures Technology*; Editors: M. Tomizuka, B.F. Spencer, C.B. Yun, W. Chen, R. Chen; Taylor & Francis Ltd, 2008.

[5] R.C. Barros and O. Corbi, "Computational and Experimental Developments of Vibration Control using Liquid Tanks for Energy Dissipation Purposes in Civil Engineering Structures", Proceedings of ECCOMAS Thematic Conference "*Computational Methods in Structural Dynamics and Earthquake Engineering* (COMPDYN 2007)", Ed.: M. Papadrakakis, D.C. Charmpis, N.D. Lagaros, V. Tsompanakis; Rethymno, Creta (Greece), 13-16 June 2007, Book of Abstracts pp. 268, Full paper 1732 - 13 pages, 2007.

[6] Rui Carneiro de Barros and Ottavia Corbi, "An Overview on Some Ongoing Computational and Experimental Campaigns on Vibration Control by Liquid Tanks", *International Journal of Mechanics and Solids*, ISSN 0973-1881, Volume 3, Number 1, pp. 1-22, Research India Publications, India, 2008.

[7] L. Guerreiro, R.C. Barros and R. Bairrão; "Algorithms for Semi-Active Devices Control", Proceedings of ECCOMAS Thematic Conference "*Computational Methods in Structural Dynamics and Earthquake Engineering* (COMPDYN 2007)", Ed.: M. Papadrakakis, D.C. Charmpis, N.D. Lagaros, V. Tsompanakis; Rethymno, Creta (Greece), 13-16 June 2007, Book of Abstracts pp. 262, Full paper 1733 – 6 pages, 2007.

[8] R. Bairrão, R.C. Barros and L. Guerreiro; "Shaking Table Tests in the Aim of Project COVICOCEPAD" (Comparison of Vibration Control in Civil Engineering Using Passive and Active Dampers), Proceedings of ECCOMAS Thematic Conference "*Computational Methods in Structural Dynamics and Earthquake Engineering* (COMPDYN 2007)", Ed.: M. Papadrakakis, D.C. Charmpis, N.D. Lagaros, V. Tsompanakis; Rethymno, Creta (Greece), 13-16 June 2007, Book of Abstracts pp. 260, Full paper 1731 – 5 pages, 2007.

[9] C.F. Oliveira, R. Bairrão, R.C. Barros and L. Guerreiro; "The New Generation of Seismic Semi-Active and Active Protection Systems"; *4th European Conference on Structural Control* (4ECSC), Paper 227, St Petersbourg, Russia, 8-12 September 2008.

[10] R. Bairrão, L. Guerreiro and R.C. Barros; "Shaking Table Tests on Semi-Active Tuned Mass and Tuned Liquid Dampers"; *14 WCEE*, Beijing, China, 12-17 October 2008.

[11] A. Baratta, I. Corbi and O. Corbi; "On the Dynamics of Unilaterally Supported Rigid Blocks", *14 WCEE*, Beijing, China, 12-17 October 2008.

[12] F. Naeim and J.M. Kelly, *Design of Seismic Isolated Structures*: from Theory to Practice, John Wiley & Sons Inc., New York - USA, 1999.

[13] T.T. Soong and G.F. Dargush, *Passive Energy Dissipation Systems in Structural Engineering*, John Wiley & Sons Ltd, Chichester - England, 1999.

[14] R.C. Barros and M.B. César, "Seismic Behaviour of an Asymmetric Three-Dimensional Steel Frame with Base Isolation Devices"; in: *Computational Structures Technology*; Editors: B.H.V. Topping, G. Montero and R. Montenegro; Paper 252, Civil-Comp Press, Stirlingshire, Scotland, 2006.

[15] M.B. César and R.C. Barros, "Influence of Resistant Cores Location on the Seismic Response of a R/C 3D-Frame Equipped with HDRB Base Isolation Devices"; in: *Civil Engineering Computing*; Editor: B.H.V. Topping; Paper 199, Civil-Comp Press, Stirlingshire, Scotland, 2007.

[16] E. Figueiredo and R.C. Barros, "An Insight on the Influence of Damping in Seismic Isolation", in: *Civil Engineering Computing*, Editor: B.H.V. Topping, Civil-Comp Press, Paper 201, Civil-Comp Press, Stirlingshire, Scotland, 2007.

[17] A. Baratta and I. Corbi, "On the optimal design of structural base isolation devices"; in: *Computational Mechanics*: 283-285; Edts: E. Lund, N. Olhoff, J. Stegmann; Aalborg University, Denmark, 2002.

[18] A. Baratta and I. Corbi, "Optimal design of base-isolators in multi-storey buildings". *Int. J. Computers & Structures*, vol. 82, Issues 23-26: 2199-2209, Elsevier, 2004.

[19] A. Kareem, "Next Generation of Tuned Liquid Dampers", *Proc. First World Conf. on Structural Control*, Vol. 3 : pp. 19-28, International Association for Structural Control, Los Angeles, 1994.

[20] O. Corbi, "Experimental Investigation on Sloshing Water Dampers Attached to Rigid Blocks", *Proc. 5th Wseas Int. Conf .Applied Comp. Science*, Hangzhou**,** China, 2006.

[21] R.C. Barros, *Seismic Analysis and Design of Bottom Supported Anchored Metallic Tanks*, Edições INEGI - Instituto Engenharia Mecânica e Gestão Industrial, ISBN: 978-972-8826-18-5, FEUP, Porto, Portugal, 2008.

[22] S.J. Dyke, B. F. Spencer, M.K. Sain, and J.D. Carlson; "Modeling and control of magnetorheological dampers for seismic response reduction", *Smart Materials and Structures*, Vol. 5, pp. 565-575, 1996.

[23] L.M. Jansen and S.J. Dyke, "Semi-active control strategies for MR dampers: A comparative study", *ASCE Journal of Engineering Mechanics*, Vol. 126, No. 8, pp. 795-803, 1999.

[24] C. Kang-Min, C. Sang-Won, J. Hyung-Jo and L. In-Won; "Semi-active fuzzy control for seismic response reduction using magnetorheological dampers", *Earthquake Engineering and Structural Dynamics*, Vol. 33, pp. 723-736, John Wiley & Sons, Ltd., 2004.

[25] C. Oliveira and L. Guerreiro; "A Velocity and Displacement Dependent Semi-active Control Algorithm", *First European Conference on Earthquake Engineering and Seismology*, Geneva, 2006.

[26] C. Oliveira, *Dynamic Behaviour Analysis of Bridges with Adaptative Protection Systems*, PhD thesis Technical University of Lisbon, IST, Lisbon, 2008.

[27] R. Bairrão, O. Bursi, P. Carydis, G. Magonette, H. Mouzakis, D. Tirelli, M. Williams; "Benchmark Testing and Performance Comparison of Shaking Tables and Reaction Walls", *Proceedings of the 13WCEE*, Paper 441, Vancouver, Canada, 2004.

[28] Industrial Application of Shaking Tables and Reaction Walls, NEFOREEE Project, University of Trento, Italy, 2004.

[29] prEN 1998-1, "Eurocode 8: Design of Structures for Earthquake Resistance"; Part 1: general rules, seismic actions and rules for buildings; *CEN – European Committee for Standardization*, Brussels, Belgium, 2002.